

# A method to infer past surface mass balance and topography from internal layers in martian polar layered deposits

Michelle R. Koutnik<sup>a,\*</sup>, Edwin D. Waddington<sup>a</sup>, Dale P. Winebrenner<sup>a,b</sup>

<sup>a</sup>University of Washington, Department of Earth and Space Sciences, Box 351310, Seattle, WA 98195, USA

<sup>b</sup>University of Washington, Applied Physics Laboratory, Box 355640, Seattle, WA 98195, USA

## ARTICLE INFO

### Article history:

Received 20 January 2009

Revised 27 May 2009

Accepted 24 June 2009

Available online 28 June 2009

### Keywords:

Mars, Polar caps

Mars, Climate

Ices

Earth

Radar observations

## ABSTRACT

Internal layers in ice masses can be detected with ice-penetrating radar. In a flowing ice mass, each horizon represents a past surface that has been subsequently buried by accumulation, and strained by ice flow. These layers retain information about relative spatial patterns of accumulation and ablation (mass balance). Internal layers are necessary to accurately infer mass-balance patterns because the ice-surface shape only weakly reflects spatial variations in mass balance. Additional rate-controlling information, such as the layer age, the ice temperature, or the ice-grain sizes and ice-crystal fabric, can be used to infer the absolute rate of mass balance. To infer mass balance from the shapes of internal layers, we solve an inverse problem. The solution to the inverse problem is the best set or sets of unknown boundary conditions or initial conditions that, when used in our calculation of ice-surface elevation and internal-layer shape, generate appropriate predictions of observations that are available. We also show that internal layers can be used to infer martian paleo-surface topography from a past era of ice flow, even though the topography may have been largely altered by subsequent erosion. We have successfully inferred accumulation rates and surface topography from internal layers in Antarctica. Using synthetic data, we demonstrate the ability of this method to solve the corresponding inverse problem to infer accumulation and ablation rates, as well as the surface topography, for martian ice. If past ice flow has affected the shapes of martian internal layers, this method is necessary to infer the spatial pattern and rate of mass balance.

© 2009 Elsevier Inc. All rights reserved.

## 1. Introduction

The spatial pattern and rate of accumulation and ablation (mass balance) over an ice cap (i.e. mass exchange with the atmosphere) must be known in order to infer the ice-flow history. On Earth, rates of accumulation can be determined by drilling an ice core, measuring the thickness of datable layers, and correcting for strain thinning where necessary, but this represents mass-balance conditions at only the single point of origin of each ice-core sample. Internal layers, which in almost all terrestrial cases are isochrones, contain information about mass-balance patterns in both space and time. The large body of radar data from terrestrial ice sheets has greatly increased our understanding of terrestrial ice-sheet evolution and climate (e.g. Paren and Robin, 1975; Morse et al., 1998; Conway et al., 1999; Fahnestock et al., 2001).

Past and present accumulation and ablation rates are fundamental unknowns for the martian polar layered deposits (PLD). This information is necessary if we are to decipher the connection between climate and PLD formation, evolution, and observable

structure. Internal-layer shapes must be known if we want to determine past mass-balance patterns, because the surface topography is relatively insensitive to spatial variations in mass balance. Fortunately, internal layers in the North and South PLD have been imaged successfully by radar (e.g. Picardi et al., 2005; Plaut et al., 2007; Seu et al., 2007; Phillips et al., 2008).

While present-day ice flow on Mars may have an insignificant influence on the shape of the PLD, it has been proposed that ice flow was more important in the past (e.g. Clifford, 1987; Fisher, 2000; Pathare and Paige, 2005), and Winebrenner et al. (2008) showed that the shape of present-day inter-trough topography along lines following surface gradients (i.e. “flowlines”) across Gemina Lingula (also referred to as Titania Lobe; Pathare and Paige, 2005), North PLD matches the shape of an ice mass that has flowed. We consider an era of past ice flow as a time when the influence of ice flow was comparable to the influence of mass balance in shaping the internal layers and the ice-surface topography. In this paper, we assume that past ice flow affected the shapes of internal layers and the surface topography of the martian PLD. Under this assumption, an approach that accounts for the effect of ice flow on the internal-layer shape and depth must be used to infer the mass-balance pattern from internal layers; we demonstrate such

\* Corresponding author. Fax: +1 206 543 0489.

E-mail address: [mkoutnik@ess.washington.edu](mailto:mkoutnik@ess.washington.edu) (M.R. Koutnik).

a method here. In addition, we emphasize that the shapes of internal layers alone cannot be used to determine whether an ice mass has flowed or not; this is discussed more fully in Section 3.3. Depending on the spatial pattern of accumulation and ablation, identical layer shapes can be generated in an ice mass where flow is significant and in an ice mass where flow is insignificant relative to other processes. Conversely, flowing ice masses with similar surface topography but different accumulation patterns can have dramatically different internal-layer architecture.

Using terrestrial glaciological experience and methods that have been applied to terrestrial ice sheets, we show that an inverse method can potentially infer mass-balance patterns during that era of flow, from internal-layer shapes on Mars. To demonstrate this method, we generate synthetic internal layers based on a prescribed spatial mass-balance distribution, and then we attempt to infer the mass-balance pattern from these synthetic layers. The *relative mass-balance pattern* can be successfully inferred from the shapes of internal layers; however the layer age, the ice temperature, the ice velocity, or the ice-grain sizes and ice-crystal fabric must be known to constrain the *absolute mass-balance rate*.

We solve different inverse problems to infer mass balance by assuming that different combinations of information are available. In the first inverse problem, we infer only the relative spatial pattern of mass-balance from the shape of an internal layer with no rate information. This problem could potentially be solved with data currently available for Mars. Then we solve three different inverse problems to infer the relative spatial pattern and the absolute rate of mass-balance in a flowing ice mass. We use (1) the ice-surface topography and ice temperature, (2) the shape of an internal layer, the ice-surface topography, and ice temperature, or (3) the shape of an internal layer, the ice-surface topography, and ice-rheological parameters. Finally, we also solve an inverse problem using internal layers to infer surface topography from a time in the past when ice flow significantly shaped the surface; this is an important problem to solve with martian internal layers because much of that topography has been significantly eroded to form the present-day surface.

### 1.1. Internal-layer structure and depth

In a flowing ice mass, the depth variations of an individual internal layer are controlled by the spatial pattern of mass balance, and by ice flow. Waddington et al. (2007) discussed how to diagnose the appropriate strain regime of a particular layer. Shallow layers (with a depth of at most a few percent of the ice thickness, or in the upper tens of meters in a terrestrial ice sheet), are not significantly altered by ice flow, and the net accumulation at each site can be inferred from the ice-equivalent layer depth divided by the layer age; this is called the Shallow Layer Approximation (SLA). For shallow layers, the mass-balance pattern alone determines the internal-layer structure and depth. If the influence of mass-balance on the shapes of internal layers was always more important than the influence of ice flow, the SLA would be appropriate for layers at all depths. However, in a flowing ice mass, as the depth to the layer increases, accumulated strain due to ice flow becomes more important, and this simple SLA relationship between layer depth and the mass-balance pattern breaks down. For intermediate layers (in the upper 10–20%, or to a depth from 10 to 100 m in a terrestrial ice sheet), the impact of accumulated vertical strain on the depth of the layer can be estimated using a 1-D model of vertical ice flow; this is called the Local Layer Approximation (LLA). However, this local strain correction also can become invalid for deeper layers. Deeper, older layers reflect conditions further in the past, but they have been more affected by horizontal gradients in strain rate and accumulation. Therefore, their information is highly valuable but more difficult to interpret. Waddington et al. (2007) dem-

onstrated that it is necessary to use formal inverse methods, incorporating 2-D ice flow, to correctly determine the accumulation pattern recorded by deeper layers in terrestrial ice caps. We cannot rule out that ice flow was important in shaping topography and internal structure across the PLD, especially for Gemina Lingula, North PLD (Winebrenner et al., 2008). Therefore, we expect that an inverse method must be used to infer spatial patterns and rates of mass-balance from deeper layers in martian ice.

On terrestrial glaciers, and parts of the large terrestrial ice sheets, snow typically accumulates at higher elevations (the accumulation zone). Ice flow redistributes the excess mass to lower elevations where it ablates (the ablation zone). The equilibrium line demarcates the two zones. Internal horizons represent past ice-sheet surfaces, which have been subsequently buried, and the thickness of ice between any two horizons has been displaced and strained by ice flow. On Earth and Mars, we assume that each individual horizon is an isochrone, i.e. a surface of constant age. The horizons are observed with ice-penetrating radar, and at different depths there are different distances between each pair of horizons. In this paper we refer to each horizon as a ‘layer’, but we note that a layer also has a thickness. The shape and depth of an individual layer are influenced by the rate of accumulation or ablation, gravitational forces, internal stresses, ice-rheological parameters (which depend on the ice temperature), bedrock topography, and unconformities.

### 1.2. Necessary data

Internal layers have been observed across the martian PLD by the Mars Advanced Radar for Subsurface and Ionosphere Sounding (MARSIS; e.g. Picardi et al., 2005; Plaut et al., 2007) and by the Shallow Subsurface Radar (SHARAD; e.g. Seu et al., 2007; Phillips et al., 2008). The shapes of continuous internal layers along putative flow lines will be the primary data when we apply our method to Mars in the future. We also use the PLD surface geometry, which is available from the Mars Orbiter Laser Altimeter (MOLA), and the ice thickness from the radars. Currently, the internal-layer ages, the ice velocity at the time of flow, the ice temperature at the time of flow, the ice-crystal fabric, and the ice-grain size are not known for the PLD. However, if any of this information becomes available, or can be reasonably estimated, then we can incorporate it as part of the inverse problem.

## 2. Methods

Inference of mass-balance patterns from internal layers is an inverse problem, which can be solved using geophysical inverse theory (e.g. Menke, 1989; Parker, 1994; Aster et al., 2005). An inverse problem is one where the existing data have resulted from a known process that depends on some unknown parameter values or boundary conditions that we wish to find. In the martian problem, the data are the shapes of individual internal layers and at least parts of the elevation profile of the ice surface, and the unknowns are the layer ages, the mass-balance pattern, and the ice temperature. An inverse problem needs a forward algorithm and an inverse algorithm. We calculate the shapes of layers and the surface topography with the forward algorithm. Then the unknown parameters can be found by minimizing a performance index in the inverse algorithm. The performance index is a number representing how well the observable quantities calculated by the forward algorithm match the data to an expected tolerance while, in this case, finding a spatially smooth mass-balance pattern. Any simplifications made in the forward algorithm, or constraints included in the inverse algorithm, must be considered when interpreting the solution.

In Appendix A we describe our particular forward algorithm, and in Appendix B we outline our particular inverse algorithm. The forward algorithm is a steady-state flowband model that calculates ice-surface elevation and internal-layer shapes (Waddington et al., 2007). A flowband is illustrated in Fig. 1. This is a 2-D model that also accounts for width variations; therefore it is considered to be 2.5-D. There are many unknowns regarding the martian PLD, and for this reason we start with a simple, steady-state forward model. As shown in Fig. 1, the model domain does not need to include an ice-sheet terminus or an ice divide; it can be defined over a limited domain. The surface-profile prediction depends on the ice flux entering the domain, the mass-balance profile, the ice thickness at one point in the domain, and the constitutive properties of the ice. Layer prediction in this forward calculation requires the ice-surface profile, which is either known or calculated, and depends on the layer age, the ice flux entering the domain, and the mass-balance pattern. The forward algorithm can include only a surface calculation, only a layer calculation, or both a surface calculation and a layer calculation (see Appendix A). Therefore, our unknown model-parameter set may consist of the layer age, the ice flux entering the domain, the spatial pattern of mass balance, the ice thickness at one point in the domain, and the ice-softness parameter (see Eq. (A.5)). The inverse algorithm uses a Gradient solution method (e.g. Parker, 1994; Aster et al., 2005) to find physically reasonable values of these unknown parameters (see Appendix B). The preferred parameters generate an internal layer and an ice surface that fits the data at an expected tolerance determined by data uncertainties.

This general method can be modified based on site-specific conditions and/or data availability. Following Waddington et al. (2007), we illustrate this method using data from Antarctica. In preparation for using this method with martian radar data, we generate synthetic martian layers, and then we investigate the ability of the inverse procedure to infer a known synthetic mass-balance pattern from those synthetic layers.

### 3. Results

Depending on which data are available, and which calculations are included in the forward algorithm, different quantities must be assumed, and different information can be inferred with this inverse approach. The simplest problem uses a forward algorithm that includes only a kinematic layer calculation, assuming that the surface topography is known, to infer the relative mass-balance pattern from an undated internal layer. We show that if the layer age is known, or if the ice velocity or the accumulation rate during the era of flow is known, we can also infer the absolute mass-balance rate using a forward algorithm that includes only a kinematic

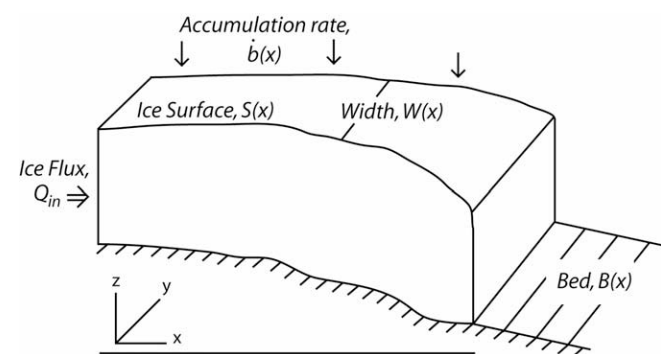


Fig. 1. Geometry of a flowband with width variations. The ice-surface elevation (at least at a single point), flowband width, and bed geometry are required inputs to the forward algorithm. The flowband domain can be limited in horizontal extent.

calculation. In principle, data that are currently available for Mars could be processed along flowlines so that some of the inverse problems here could be solved. The other problems further motivate challenges for future laboratory experiments and missions.

Using steady-state continuity from Eq. (A.1), and using the depth-averaged horizontal velocity in Eq. (A.6), Eq. (1) shows how, for any ice-sheet profile defined by the ice thickness  $H(x)$  and surface slope  $dS/dx$ , the accumulation rate  $\dot{b}(x)$  and the ice-temperature-dependent softness parameter  $A(T(x))$  always occur in a ratio,

$$\left[ \frac{\dot{b}(x)}{A(T(x))} \right] = \frac{1}{x} \frac{2}{n+2} (\rho g)^n \left| \frac{dS}{dx} \right|^{n-1} \left( -\frac{dS}{dx} \right) H^{n+2} W(x). \quad (1)$$

Higher accumulation rates  $\dot{b}(x)$  can always trade-off against greater ice softness  $A(T(x))$  through higher temperature, to produce the same surface shape, and therefore the same layer shape with a younger layer age. We discuss ways in which accumulation rate and ice temperature may be untangled.

#### 3.1. Mass balance and topography in Antarctica

Waddington et al. (2007) solved the inverse problem to infer the relative spatial pattern and absolute rate of accumulation at Taylor Mouth, a flank site near Taylor Dome, Victoria Land, Antarctica. At Taylor Mouth, additional data were available beyond the surface topography and internal-layer shapes observed with radar. Bed elevation was also measured by radar, and flowband width was found by interpolating velocities between measurement points and finding the distance between two nearby flow lines. A 100-m ice core intersects the flow line, and the average accumulation rate at the core site was known. A strain network in this area provided velocity data at the ice surface.

The forward algorithm in this previous application to Taylor Mouth (Waddington et al., 2007) included only a kinematic layer calculation. The unknown parameter set consisted of the ice flux entering one end of the flowband, the spatial pattern of accumulation (there is no ablation area near this site), and the age of the layer. Use of only a kinematic forward algorithm was justified because the surface elevation at Taylor Mouth has been approximately in steady-state over the past few thousand years. Therefore, the dynamic calculation of surface topography could be excluded to simplify the problem. Since the surface topography is known, and because a dynamic calculation was excluded in the forward algorithm, rate information was included only through the surface-velocity measurements and the one accumulation-rate measurement. At Taylor Mouth, these rate-containing data were sufficient to constrain the magnitude of accumulation rate.

##### 3.1.1. Inferring mass balance from an undated layer

To show the sensitivity of the Taylor Mouth solution (Waddington et al., 2007) to rate information from measurements of surface-velocity and accumulation rate, and to prepare for martian applications where rate information is unavailable, we now solve the Taylor Mouth inverse problem using only internal-layer data. In this problem, the mass-balance rate is determined by the layer age. If the internal layer is undated, and if no additional rate-controlling data exist, we can infer only the relative mass-balance pattern. To express this result, we represent the spatial pattern of accumulation,  $\dot{b}(x_i)$  at spatial positions  $x_i$ , as a non-dimensional spatial pattern of accumulation,  $\tilde{b}(x_i)$ , having root-mean-square amplitude, i.e.

$$\frac{1}{L} \int_0^{x=L} \tilde{b}^2(x) dx = 1, \quad (2)$$

multiplied by the magnitude  $B$  of the accumulation rate, giving

$$\dot{b}(x_i) = B\dot{\tilde{b}}(x_i). \quad (3)$$

By representing the mass-balance pattern  $\dot{b}(x_i)$  in this way, we can compare the values of  $B$  that correspond to solutions using different combinations of rate-controlling data (e.g. the layer age or the ice temperature).

Fig. 2a shows different accumulation-rate solutions corresponding to differing guesses of the layer age, inferred using only an internal layer as data, and using the known modern surface topography. Particles can follow the same paths and reach the same depths over a longer time when accumulation rate is low, or over a shorter time when accumulation rate is high. The central result from this test is that similar spatial patterns can be inferred, regardless of the accumulation-rate magnitude. Fig. 2b shows  $B/B_{ref}$ , the scaling factor  $B$  divided by the scaling factor of a reference solution  $B_{ref}$  (here taken to be the solution from Waddington et al. (2007)), corresponding to the solutions in Fig. 2a.

On Mars, we are likely to know only the layer shape. It is unlikely that we will know the layer age, and velocities and accumulation rates from the regime in which the layers formed cannot be measured. However, by exploring the sensitivity of the Antarctic solution, we found that useful information about the relative spatial variability in mass balance can still be inferred, even if the absolute rate of accumulation cannot be recovered.

### 3.1.2. Inferring surface topography

We can also infer the shape of the ice-surface topography from the shape of an internal layer. This will be useful for the PLD, where the surface shape at the time of flow has been subsequently eroded, or largely obliterated. We demonstrate this using data from Taylor Mouth, Antarctica.

If the surface topography is unknown, and is being solved for as part of the inverse problem, we still have to estimate the surface topography for the first iteration of the forward algorithm. As the inferred mass-balance pattern is iteratively updated in the inverse algorithm, the inferred surface topography is also updated, using Eq. (A.7), and this updated surface is used in the subsequent itera-

tion for the mass-balance pattern. The unknown parameter set consists of the ice flux entering one end of the flowband  $Q_{in}$ , the spatial pattern of accumulation  $\dot{b}(x)$ , the age of the layer  $Age$ , and the ice thickness at one location along the flowband  $H_0$ . In the absence of rate-controlling information (e.g. layer age, ice velocity), we have shown that we cannot determine the absolute rate,  $B$ , of mass balance.

Using data from Taylor Mouth, Antarctica, we demonstrate our ability to infer the ice-surface topography by performing two tests. First, we infer ice-surface topography from the shape of an undated internal layer, an estimate of elevation at one point on the ice surface, and the known ice temperature (referred to as test 1). We estimate the ice-surface elevation at the furthest upstream point along the flowband and assume that we know this value within 5 m. In this problem, with no additional rate-controlling data, the ice temperature determines the inferred mass-balance rate and the length of the ice mass (the maximum thickness is specified).

In the second test (referred to as test 2) we infer ice-surface topography from the shape of an undated internal layer and at least two points on the ice surface. We assume that the ice temperature is unknown, and the greater the horizontal distance between the two known surface-elevation points, the better we can infer the ice-surface profile. We show that we can infer a surface with the correct shape, even if the inferred rates are incorrect. At the first iteration of the forward algorithm we guess that the ice-surface has a uniform elevation along the flowband. We guess that the ice-softness parameter  $\dot{A}(x)$  is five times greater than the original value, so that the deformation rates are five times larger. The inferred mass-balance pattern together with the inferred ice-surface shape generate an internal layer that has the appropriate balance between smoothness and fit to the data, where the data are fit with a root-mean-square mismatch consistent with data uncertainties (see Appendix B).

Fig. 3a shows that the solution from the inverse problem is similar to the actual ice surface at Taylor Mouth (dotted line). Fig. 3b compares the mismatches of tests 1 and 2 against the actual ice surface, normalized by a reasonable estimate of the measurement uncertainty of 5 m. This test with Taylor Mouth data shows that

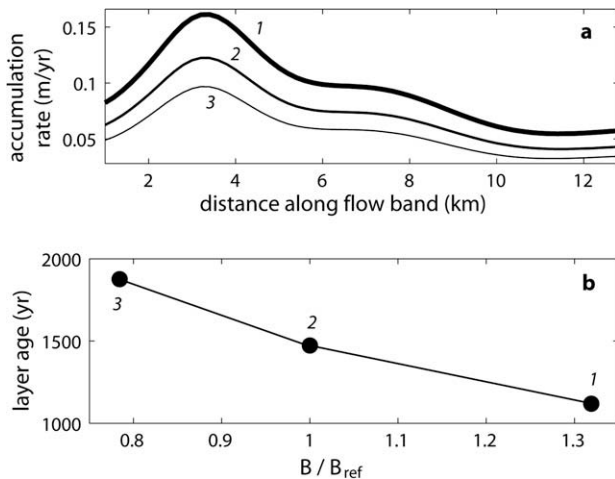


Fig. 2. (a) The accumulation-rate solution for the Taylor Mouth inverse problem using an undated internal layer and no rate-controlling data. The dark gray line shows the solution with an initial guess at the layer age that was 25% lower (resulting in a higher accumulation rate) than the layer age inferred from Waddington et al. (2007), and the light gray line shows the solution with an initial guess at the layer age that was 25% higher (resulting in a lower accumulation rate). (b) The numbered points correspond to the numbered solutions in the above panel. The accumulation-rate magnitude  $B$  equals unity for the correct accumulation rate. Without additional rate information, the same internal layer can be generated with an older age and a lower accumulation rate, or a younger age and higher accumulation rate.

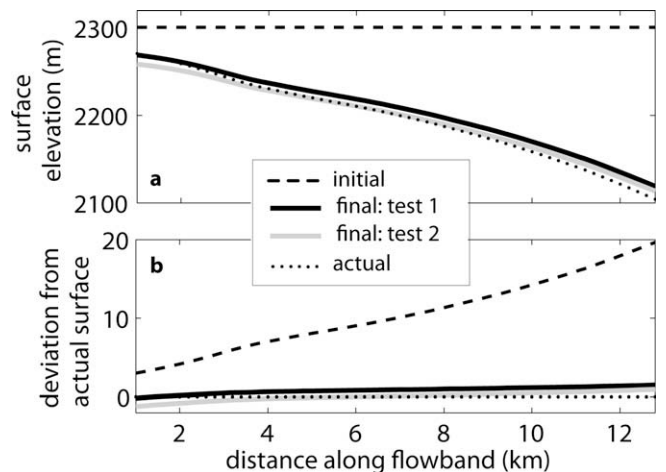


Fig. 3. (a) Comparison between the actual ice-surface topography at Taylor Mouth, Antarctica (dotted line), the initial guess of ice-surface topography (dashed line), and the best estimate of ice-surface topography found by solving the inverse problem using an internal layer, the ice-surface elevation at one point, and a known ice temperature (test 1; black-solid line), and using an internal layer and two points on the ice surface (test 2; gray-solid line). (b) The actual ice surface is subtracted from itself (dotted line), from the ice-surface topography estimated at the initial iteration (dashed line), and from the ice surface found by solving the inverse problem (black and gray-solid lines), all nondimensionalized by the uncertainty of 5 m in the measured surface elevation.

the surfaces found by solving these inverse problems have the same shape as the measured surface; this is a significant result. The inferred values are within one standard deviation of the point(s) on the surface that are known, and at most within two standard deviations elsewhere along the profile. Knowledge of the ice temperature, especially if there are spatial variations in ice temperature, gives a slightly better solution. However, since ice-temperature information is not currently available for Mars, it is important that we can infer the shape of the surface topography from an internal layer and two points on the ice surface; in Section 3.4.5 we discuss a test to reconstruct paleo-surface topography using synthetic data for Mars.

### 3.2. Synthetic data for Mars

To demonstrate the usefulness of our inverse approach, we solved inverse problems with synthetic “data” that we generated for Mars. Using our forward algorithm with prescribed maximum ice thickness, ice-softness parameter, mass-balance pattern, layer age, and input ice flux at the upstream end of the flowband, we calculated the associated ice-surface profile and generated shapes of synthetic internal layers. Then we used these synthetic data with our inverse method to infer a model-parameter set that included a characteristic ice thickness, the ice-softness parameter, the mass-balance pattern, the layer age, and the input ice flux. In order to see how well our inverse procedure worked, we compared the inferred set of model parameters to the known values that we used to generate the synthetic data.

The following assumptions were made in all our tests for the PLD. The modeled PLD were assumed to be pure ice, which restricts the value of the softness parameter  $A_0$  (in Eq. (A.5)). The exponent in the constitutive relationship for ice flow, Eq. (A.4), had a value of  $n = 3$ , as inferred by Winebrenner et al. (2008) for martian ice. An exponent of  $n = 3$  is typical for terrestrial ice sheets and applies for deformation primarily by dislocation creep (e.g. Paterson, 1994, p. 85). The temperature at depth was approximated by a uniform gradient using a surface temperature of 170 K (e.g. Pathare and Paige, 2005) and a basal heat flux of  $0.025 \text{ W m}^{-2}$  (e.g. Clifford, 1987; Grott et al., 2007). The maximum ice thickness and bed topography used to generate synthetic data resemble conditions on the present-day North PLD (e.g. Phillips et al., 2008), as does our chosen mass-balance rate of  $\sim 0.5 \text{ mm year}^{-1}$  (e.g. Laskar et al., 2002). Present-day ice temperatures (e.g. Pathare and Paige, 2005) make ice flow very slow, but any value of ice temperature could have been used. The surface geometry for each mass-balance pattern came from a steady-state surface calculation based on ice dynamics using Eq. (A.7). The ice-divide thickness was chosen to be 2 km. We assume a uniform flowband width, which is a simplification, and the flowband width could be estimated by tracking the divergence of adjacent flow paths along the surface of the actual topography, as done by Winebrenner et al. (2008).

Using our estimate of surface temperature, heat flux, and mass-balance rate, and because the steady-state model does not allow for past ice-temperature transients, the resulting length of the flowband is approximately 20 km, and we can solve the inverse problems using only a limited portion of this full length. Compared to modern flowband lengths of  $\sim 100 \text{ km}$  or more across the PLD, these lengths are very short because near-basal ice at the present-day temperature of  $\sim 180 \text{ K}$  (e.g. Pathare and Paige, 2005) requires very steep slopes to achieve equilibrium with the present-day mass balance of  $\sim 0.5 \text{ mm year}^{-1}$  (e.g. Laskar et al., 2002). Present-day ice is so cold that ice-flow rates are insignificant with the existing low surface slopes (e.g. Hvidberg, 2003; Greve et al., 2004; Greve and Mahajan, 2005), and conditions must have been different in the past for ice flow to shape the observed topography (Winebrenner et al., 2008; Koutnik et al., 2008). The

bed topography was chosen to be flat, but any topography can be used in the model. We used an isothermal temperature distribution, and we assigned an age of 1 Myr to the synthetic data layer. To make the inverse problem more realistic, we added red noise to our synthetic layer and used the perturbed layer as the data. We set the standard deviation,  $\sigma_i^{(d)}$ , on the layer data to be 3 m because we applied red noise with an amplitude of 3 m, and chose a correlation length of 600 m. Our initial guess at the layer age was several percent higher than the true age of the synthetic data; any initial guess could be used. The initial guess of the accumulation rate was the layer depth divided by our initial guess of the layer age (SLA, see Section 1.1). We focused our study near the ice divide, where no ice flux enters the domain (i.e.  $Q_{in} = 0$ ).

### 3.3. Internal-layer shapes

Internal-layer shapes can be generated for any mass-balance pattern and flow regime. For example, Fisher (2000) generated internal-layer shapes for the “accublation” model (Fisher, 1993, 2000). The accublation mass-balance pattern has alternating zones of accumulation and ablation to account for the presence of troughs on the North PLD landscape. In the accublation model, the shapes of both the ice surface and the internal layers were significantly affected by the mass-balance pattern. However, it is also possible for different mass-balance patterns to result in similar surface profiles, yet have very different internal-layer shapes (see Fig. 5).

While the mass-balance pattern directly shapes the internal layers, the surface shape is relatively insensitive to details of the mass-balance pattern. The ice flux  $q(x)$ , given by Eq. (A.2), is proportional to the integral of the mass-balance pattern. The surface slope, given by Eq. (A.7), is smooth because it depends on the mass-balance pattern only through the  $n$ th-root of the ice flux,  $q(x)^{1/n}$ . The surface slope is integrated to get the ice-surface topography, which further reduces the influence of mass-balance variability on the ice-surface topography.

#### 3.3.1. Synthetic mass-balance patterns

We generate steady-state internal layers over a limited part of the domain using several different mass-balance patterns to emphasize the variation of internal-layer shapes. Fig. 4 shows layers generated with a synthetic mass-balance pattern with linearly decreasing accumulation transitioning into linearly increasing ablation as elevation decreases. The equilibrium line marks the point of balance between net accumulation and net ablation. Layers near the ice divide in this accumulation zone can have simple, nearly horizontal shapes. Since the transition from net accumulation to net ablation is continuous, the internal layers trend gradually toward the surface, and can intersect the surface in the ablation zone. In this example, layers also trend towards the surface in the accumulation zone because the accumulation rate decreases with decreasing surface elevation. Even though the magnitude of ablation is small, ablation has a significant impact on the layer shape.

Fig. 5 shows layers generated with a more complicated mass-balance pattern that fluctuates on smaller spatial scales. The internal-layer shapes reflect these smaller-scale variations in mass balance, but as expected, the ice surface is insensitive to these details. The gray-dashed line in Fig. 5 shows the ice surface generated with the mass-balance pattern from Fig. 4. While the internal-layer shapes associated with the different mass-balance patterns in Figs. 4 and 5 are very different, the ice-surface profiles are nearly the same. We use the mass-balance pattern in Fig. 5 to illustrate how complex layer structures, including unconformities, can form in a steady state. In Section 3.4.3 we infer the mass-balance pattern using the internal layer shown in bold in Fig. 5. In

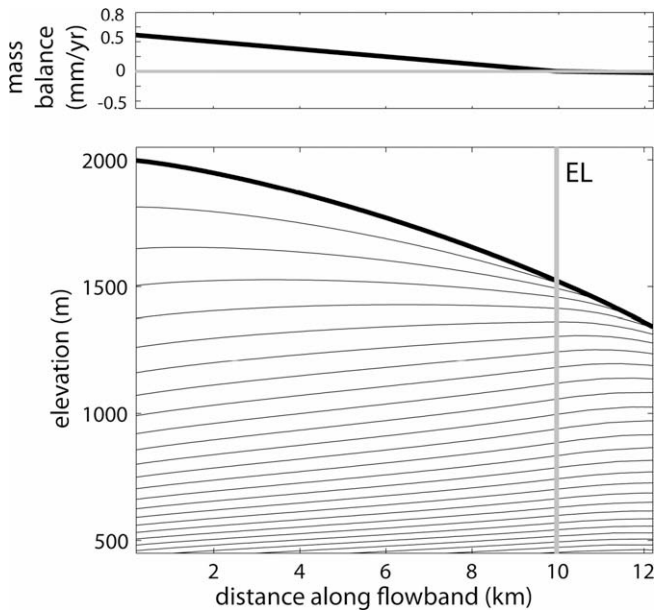


**Fig. 4.** Lower panel shows synthetic internal layers from the prescribed mass-balance pattern shown in the top panel. The mass balance decreases linearly with decreasing surface elevation, as net accumulation transitions into net ablation. The layers intersect the surface in the ablation zone. The accumulation and ablation zones are separated at the equilibrium line (EL). The bed is at zero meters, and layers are shown at equal age intervals.

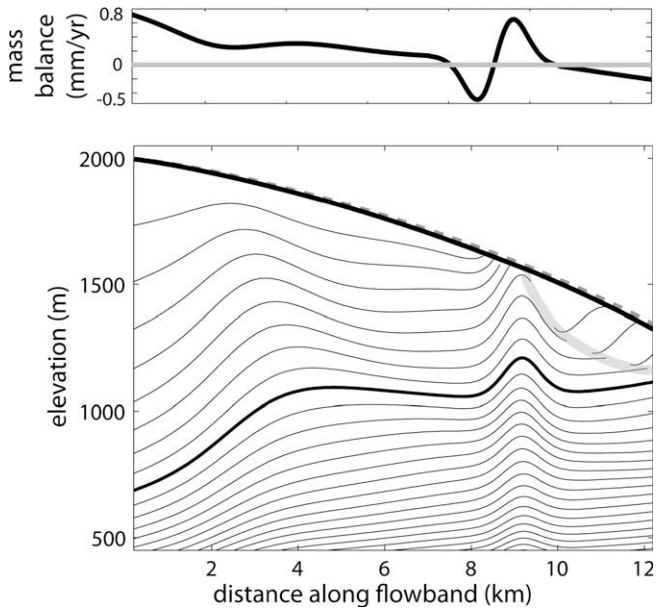


**Fig. 5.** Lower panel shows synthetic internal layers from the prescribed mass-balance pattern shown in the top panel. The mass balance varies on short spatial scales and the layers intersect the surface in the ablation zones. The bed is at zero meters, and layers are shown at equal age intervals. The unconformity, highlighted by the gray band, develops in steady state. The gray-dashed line is the ice-surface topography from Fig. 4. The shapes of the internal layers depend strongly on the mass-balance pattern, while the shape of the ice surface does not. The bold layer is used in the inverse problem we solve in Section 3.4.4 and Fig. 9.

Section 4.2 we discuss this unconformity, highlighted with a gray band in Fig. 5, which develops due to localized ablation followed by renewed accumulation in the direction of flow.

In addition to the mass-balance patterns used in Figs. 4 and 5, in Section 3.3.2 we also generated internal layers using the idealized mass-balance pattern of a zone of uniform accumulation and a

zone of uniform ablation. Figs. 4–6 show that internal layers in a flowing ice mass can also have very simple shapes; folded or faulted layer shapes are not required. In terrestrial ice sheets, folded layers can be found near the base of the ice, where bed topography, shear stress, and subtle transients in the flow direction can have a large influence on the layer shapes (e.g. Hooke, 2005, p. 361). Variations in ice rheology (e.g. Thorsteinsson et al., 2003), movement of the ice divide (e.g. Waddington et al., 2001; Jacobson and Waddington, 2005), and advance and retreat of the ice margin (e.g. Hudleston, 1976) can also cause folded layers. Waddington et al. (2001) noted that folds may be clearly identifiable only for a very short time before they overturn, which is another reason that it is rare to observe folds in terrestrial ice sheets. Layers that exhibit faulting have experienced brittle-type deformation, which is not indicative of the creep-type deformation that is associated with ice flow. Cold temperatures promote brittle behavior, and it is possible that faults are indicators of colder ice temperatures, whereas unfaulted layers may be indicative of warmer ice temperatures. These general features of internal layers in a flowing ice mass should be considered when interpreting internal structure across the martian PLD.

3.3.2. *Gemina Lingula, North PLD*

Winebrenner et al. (2008) found that the inter-trough topography of flowbands across Gemina Lingula, North PLD, closely resembled ice-surface topography generated with a simple steady-state ice-flow algorithm. They interpreted these inter-trough regions to be areas where surface topography has survived from an earlier era in which mass movement due to ice flow balanced mass exchange at the surface. Their algorithm assumed that the mass-balance pattern consisted of a zone of uniform accumulation and a zone of uniform ablation (Paterson, 1972). As explained in Section 3.3, this is not a restrictive assumption, because surface shape is relatively insensitive to details of the mass-balance distribution. By seeking the model topography that best fits the actual inter-trough topography, they could estimate the boundary between accumulation and ablation zones (the equilibrium line) when the ice was flowing.

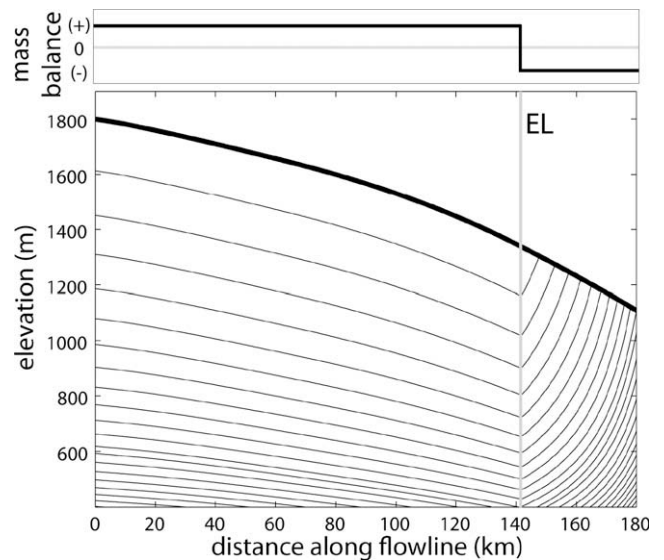


**Fig. 6.** Prediction of internal layers along a flowband on Gemina Lingula, North PLD, based on the surface topography and the idealized mass-balance pattern inferred by Winebrenner et al. (2008). The mass-balance pattern consists of a zone of uniform accumulation and a zone of uniform ablation, separated by the equilibrium line (EL).

Fig. 6 shows the internal-layer shapes corresponding to this idealized mass-balance pattern of a single zone of uniform accumulation and a single zone of uniform ablation. We cannot put a scale on this relative mass-balance pattern, because the dimensional scaling factor  $B$  (see Section 3.1.1) depends on additional assumptions about the layer ages or the ice temperature. Fig. 6 demonstrates that layers in a flowing ice mass can have simple, nearly horizontal shapes that are continuous across a broad accumulation region. In the ablation zone, layers intersect the surface. Due to the discontinuity in mass balance, the layers have a discontinuous slope at the equilibrium line, but the shape of the ice-sheet surface is smooth.

### 3.4. Past surface mass balance and topography for Mars

We demonstrate how well we can infer the model parameters by solving five different inverse problems using a uniform accumulation pattern to generate synthetic internal-layer data. In these inverse problems, in addition to the relative spatial pattern, we can infer the absolute rate of mass balance because the surface-elevation data, ice temperature, and rheological parameters may each provide rate information. For most of the inverse problems that we solve, we used a limited domain with a simple mass-balance pattern of uniform accumulation so that the results from these different inverse problems could be easily compared. However, any mass-balance pattern could be used. In Section 3.4.3, we show the results of an additional test to infer information from an internal layer generated using a mass-balance pattern that included an ablation zone; this test was done only for the case in which the data comprise only surface topography and an undated internal layer. The parameter values inferred in Sections 3.4.1–3.4.4 are compared in Table 1. The inferred mass-balance patterns are compared in Fig. 7.

#### 3.4.1. Inferring mass balance from an undated internal layer

In our first inverse problem, we attempt to infer the relative spatial pattern of mass balance  $\hat{b}(x)$ , as in Eq. (3), using a forward algorithm that adopts the synthetic surface and calculates only the internal-layer shape. This inverse problem could be solved with martian internal layers tracked along putative flowlines. This test is similar to the Antarctic example (Section 3.1.1), where the lack of data containing rate information makes it difficult to constrain the layer age; the initial guess at the layer age determines the rate of accumulation  $B$  inferred. In this test, the initial guess at the accumulation pattern differed from the known pattern, and the initial guess at the layer age was several percent higher than the known age (any age guess could be used). Even though we cannot find the correct rate, as shown in Section 3.1.1, the pattern of accumulation in the solution is a much better approximation of the true accumulation-rate pattern than our initial guess was, as shown in Fig. 7.

**Table 1**

The layer age, non-dimensional accumulation-rate magnitude  $B$  (Section 3.1.1) divided by the accumulation-rate magnitude for the correct solution  $B_{ref}$ , and the input flux for four synthetic inverse problems are compared to the correct values of the model parameters.

Inverse problem	All model parameters	Layer age, Age (Myr)	Non-dimensional accumulation-rate magnitude, $B/B_{ref}$	Input flux, $Q_{in}$ ( $m^3/year$ per m width)
Correct values of the parameters	–	1.0	1.0	0.3
Undated internal layers only	Age, $\hat{b}(x)$ , $Q_{in}$	1.13	0.88	0.261
Ice surface and known ice temperature	$\hat{b}(x)$ , $Q_{in}$ , $S_{in}$ , $A(T)$	–	1.02	0.28
Undated internal layers, ice surface, known ice temperature	Age, $\hat{b}(x)$ , $Q_{in}$ , $S_{in}$ , $A(T)$	1.0016	0.99	0.256
Undated internal layers, ice surface, known ice rheology	Age, $\hat{b}(x)$ , $Q_{in}$ , $S_{in}$ , $A(T)$ , $K$	1.002	0.98	0.35

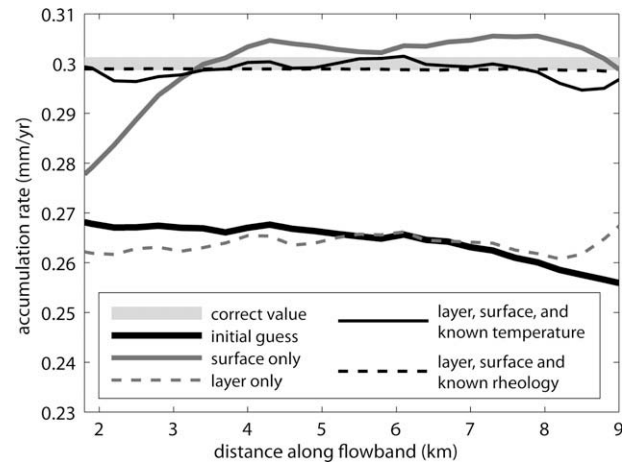


Fig. 7. The spatial patterns of accumulation from four different inverse problems are compared to each other, to the initial guess, and to the correct values (light-gray curve). Using only undated internal-layer data (gray-dashed curve) we recover the correct spatial pattern, but the wrong magnitude. Using only the surface-elevation data (dark-gray curve) we recover an accumulation-rate profile with the correct average value, but the wrong spatial pattern. Using internal-layer data and surface-elevation data, in addition to either a known ice temperature (thin solid-black curve) or known ice rheological parameters (black-dashed curve) we can recover the actual spatial pattern and rate of accumulation.

#### 3.4.2. Inferring mass balance from surface topography

In our second inverse problem, we attempt to infer the relative spatial pattern  $\hat{b}(x)$  and the absolute rate of mass balance  $B$  from the ice-surface elevation  $S(x)$  alone. As discussed in Appendix A, the surface calculation uses ice dynamics and contains rate information through the temperature-dependent ice softness parameter (Eq. (A.5)). Fig. 7 illustrates, as we anticipated, that details of the inferred mass-balance pattern are unlike the actual pattern. Using the surface data alone is not very informative about the spatial pattern of mass balance, even when the mass-balance pattern is very simple.

#### 3.4.3. Inferring mass balance with a known ice temperature

In our third inverse problem, we attempt to infer both the relative spatial pattern  $\hat{b}(x)$  and the absolute rate of mass balance  $B$  from the internal-layer shape and the ice-surface shape, assuming that the ice temperature at the time of flow is known. The results shown in Figs. 7 and 8 used the same ice temperature that was used to create the synthetic data. Using the internal layer and the ice-surface elevation as data, the inverse algorithm generates a model-parameter set that is very similar to the actual parameter values; the values are listed in Table 1. Fig. 8a shows the mass-balance solution compared to the known mass-balance pattern and an initial estimate of the mass-balance pattern from the Shallow Layer Approximation (SLA; Section 1.1) based on a poor estimate of the

layer-age parameter. Fig. 8b shows the internal-layer solution compared to the synthetic layer data, and to the initial guess of the layer calculated using an initial guess of the accumulation rate estimated from the SLA. Fig. 8c shows the paths of particles moving through the ice to form the internal layer, and Fig. 8d shows the resolving functions for this inverse problem.

Resolving functions, which indicate the ability of an inverse algorithm to resolve structure in the model parameters (see Appendix B), show that structure in the spatial variability of accumulation can be better resolved closer to the divide. The spread of the resolving functions increases due to the increasing length of particle paths further from the divide. Fig. 8c (and Fig. 9c) shows the paths of particles starting on the surface as they move through the steady-state velocity field and map out an internal layer of a particular age. Particle paths near the downstream end of the domain extend farther, and the particles can move through larger changes in accumulation and strain rate, effectively integrating information about the mass-balance pattern as they move. In addition, we desire a spatially smooth accumulation-rate solution, and we enforce this smoothness criterion in the inverse algorithm (Eq. (B.1)). Therefore, only weighted averages of accumulation rate over the width of the resolving function can be inferred.

We also generated synthetic internal-layer data with a mass-balance pattern, shown in Fig. 5, that varied on shorter spatial scales, and included an ablation zone. If an internal layer intersects the surface in the ablation zone, information about this mass-balance pattern can be inferred from that layer only over the upstream area where the internal layer exists. Fig. 9a shows the mass-balance solution compared to the known mass-balance pattern, and to the initial guess from the Shallow Layer Approximation (SLA). Fig. 9b shows the internal-layer solution compared to the synthetic layer data and the initial guess at the layer using an accumulation rate estimated from the SLA. Fig. 9c shows the paths of particles moving through the ice to form the internal layer, and Fig. 9d shows the resolving functions. Fig. 9 demonstrates that we can infer a mass-balance pattern that varied on short spatial scales; we can also recover information about the pattern of abla-

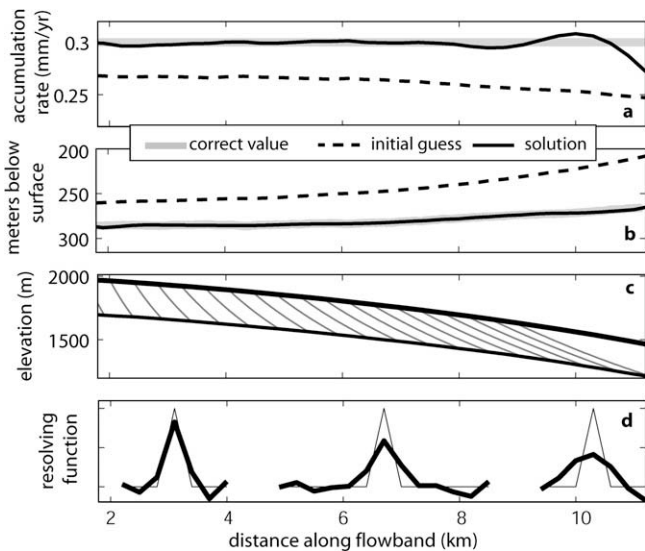


**Fig. 8.** Results for the inverse problem using an internal layer, the ice-surface shape, and a known ice temperature; a portion of this solution is also shown in Fig. 7. (a) The correct mass-balance pattern was a uniform accumulation rate of 0.3 mm year<sup>-1</sup>. (b) The synthetic data layer and the layer predicted by the forward algorithm using the model parameters were found by solving the inverse problem. (c) Paths of particles whose end points create a modeled layer. (d) The resolving function (bold line) shows the best ability of the solution to recover the single-node perturbation (thin line).

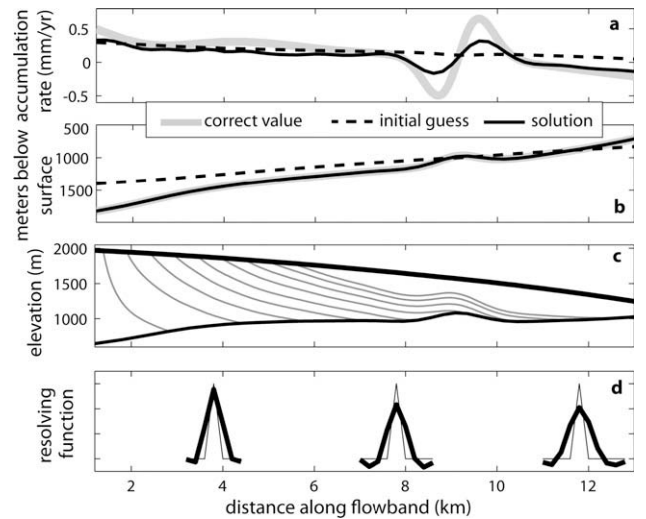


**Fig. 9.** Results for the inverse problem using an internal layer, the ice-surface shape, and a known ice temperature. (a) The correct mass-balance pattern varied on short spatial scales and included a zone of ablation. The initial guess was the depth of the layer divided by the estimated layer age. (b) The synthetic data layer and prediction by the forward algorithm using the model parameters were found by solving the inverse problem. (c) Paths of particles whose end points create a modeled layer. (d) The resolving function (bold line) shows the best ability of the solution to recover the single-node perturbation (thin line).

tion from the shape of an internal layer as it trends towards the surface. The individual influences of ice temperature and mass-balance rate are uncoupled by assuming that the ice temperature is known. For any estimate of ice temperature on Mars, the ice-surface topography and the internal-layer shape can be used to recover the corresponding absolute rate of mass balance.

### 3.4.4. Inferring mass balance with known ice rheology

In our fourth inverse problem, we attempt to infer the relative spatial pattern  $\hat{b}(x)$  and the absolute rate of mass balance  $B$  from the internal-layer shape and the ice-surface shape, assuming that the ice temperature is unknown. If both the layer age and the ice temperature are unknown, additional information must be used to uniquely determine the accumulation-rate magnitude and deformation rate, in order to infer the correct values of accumulation and ice temperature (see Eq. (1)). We demonstrate that including a third rate factor through a more general constitutive relation for strain rate may allow us to resolve both mass-balance rate and ice temperature in some circumstances.

Glen’s flow law (Glen, 1955; Eq. (A.4)) describes ice flow by a non-linear constitutive relationship between strain rate and deviatoric stress, where deformation occurs primarily by dislocation creep. The flow-law exponent,  $n$ , is typically assumed to have a value of 3. However, under different temperature and stress conditions, and for different ice-grain sizes, deformation of ice may be influenced by, or even controlled by, processes other than dislocation creep. The mechanisms of dislocation creep, grain-boundary-sliding-limited creep, and basal-slip-limited creep, can have unique flow-law exponents  $n$ , ice-grain-size exponents  $p$ , and activation energies for creep  $Q$  (Goldsby and Kohlstedt, 1997, 2001; Durham et al., 2001). In addition, the shape of an ice sheet differs when different mechanisms are dominant (e.g. Pettit and Waddington, 2003).

The stress and grain-size conditions for the different regimes in which each mechanism is dominant can be illustrated with a “deformation map” (e.g. Goldsby, 2006). Goldsby and Kohlstedt (2001) proposed a generalized flow law that explicitly accounted

for several of these deformation processes. Pettit and Waddington (2003) proposed a simpler modified flow law (discussed in Appendix C) which we use here to illustrate how the existence of multiple deformation regimes can be exploited to extract rate information. The constitutive relation in Eq. (C.1), which is a generalized version of Eq. (A.4), can account for a range of dominant deformation processes in terrestrial ice sheets, by blending  $n = 3$  processes with  $n = 1$  processes, and it can be incorporated easily into an ice-flow model. This modified flow law (Pettit and Waddington, 2003) has a second rate factor because there can be different activation energies for creep when  $n = 1$  or when  $n = 3$ , producing different temperature dependencies for  $n = 1$  and  $n = 3$  processes. When the temperature, stress, and grain size fall in a regime where both terms in the Pettit and Waddington (2003) flow law have similar magnitudes, i.e. near a boundary in a deformation map, we show that the additional rate factor can allow us to separate the individual influences of accumulation rate and ice temperature in the inverse problem, and therefore to infer both accumulation rate and ice temperature uniquely.

Using the flow law in Eq. (C.1), expressed in the form of Eq. (C.2), we solve an inverse problem with both  $\Gamma$  (defined by Eq. (C.3)) and  $k$  (defined by Eq. (C.4)) as model parameters. The parameter  $\Gamma$ , which corresponds to  $A(T)$ , given by Eq. (A.5), contains one rate factor in  $A_{01} \exp(-Q_1/RT)$ , and  $k$  incorporates another rate factor through  $A_{02} \exp(-Q_2/RT)$ , where  $Q$  is the activation energy for creep and  $R$  is the gas constant. Incorporating only one additional model parameter, the crossover stress  $k$ , instead of solving for all the rheological parameters and coefficients directly, is the simplest way to demonstrate the influence of an additional rate factor. We generated an internal layer and ice surface with  $k$  equal to  $3 \times 10^5$  Pa, using the same accumulation rate, ice thickness, and temperature from the previous synthetic tests (Section 3.3). In the inverse problem with only two rate factors (in the temperature-dependent softness parameter  $A(T)$  from Eq. (A.5), and the accumulation rate) we could not infer the correct value of the layer age and the ice temperature when both values were unknown. Many different pairs of these values could also fit the data, and the pair selected by our inverse procedure depended on our initial guesses. However, in the inverse problem with three rate factors, we can better infer the correct values of the layer age and the ice temperature in some cases when both terms in Eq. (C.2) make comparable contributions to the strain rate  $\dot{\epsilon}_{ij}$ . Table 1 and Fig. 7 show the results. The spatial pattern best matches the correct value because the crossover stress used to make the synthetic data leaves a distinct imprint on the ice-surface shape. In this case, the inferred ice-softness parameter  $\Gamma$  differs by  $\sim 1\%$  from the correct value and the crossover stress  $k$  differs by less than 3% from the correct value, compared to initial guesses that differed by 10%.

To use this additional rate factor as a constraint when solving inverse problems with martian radar data, it would be most accurate to use a generalized flow law such as that of Goldsby and Kohlstedt (2001). This requires that we know the ice-grain size (e.g. Barr and Milkovich, 2008) in the target area at the era of flow of the PLD, and the activation energies, grain-size exponents, and ice-softness parameters associated with this fully mechanism-based constitutive relationship. Not all of this information is currently available, but our synthetic tests provide another reason why they would be valuable to obtain. This is a challenge for future laboratory experiments and missions. Our synthetic test indicates that including an additional rate factor can help to constrain the timing in some cases, if the ice-rheological parameters are known, and if the ice mass is in a regime where at least two of the most important terms in the flow law (e.g. Eq. (C.2)) have a similar magnitude.

#### 3.4.5. Inferring paleo-surface topography

In our fifth inverse problem, we attempt to infer the surface topography during an era of ice flow. We have shown in Section 3.1.2 that we can successfully solve this inverse problem using data from Antarctica. The surface topography across most of the PLD has been significantly altered by trough formation, and there might not be many locations where inter-trough surface topography from a past era of ice flow is still intact (Winebrenner et al., 2008). We show how internal layers can be used to reconstruct ice-surface topography across the PLD if we can assume that there was an era of ice flow.

As in Section 3.1.2, we perform two tests of this inverse problem. First we assume that we know the elevation of one point on the ice surface and we know the ice temperature. Second, we assume that we know the elevation at two or more points on the ice surface and we do not know the ice temperature. In the first test, the surface generated with this inferred mass-balance pattern closely matched the original surface used to generate the synthetic internal-layer data. In the second test, we assume that the ice temperature is unknown, but at least two points on the ice surface are available. We find that this information about the thickness at different elevations along the flowband length allow us to reconstruct surface topography when the ice temperature is unknown. However, inferring the correct mass-balance rate  $B$  still requires correct ice-temperature information, or other rate-controlling information.

This inverse problem to infer surface topography using just two elevation-data points on the ice surface could be solved using martian internal layers tracked along putative flowlines across the PLD. Even if rate-controlling information were unavailable for the PLD, the shape of the past topography could be inferred from internal layers.

## 4. Discussion

### 4.1. Implications of ice flow

Based on our understanding of terrestrial ice masses, we expect that martian ice experiences flow at some rate. The real question is how significant this flow might be in relation to other processes. If ice flow has a minor influence on PLD structure, then both the internal-layer shape and surface shape are determined by the mass-balance pattern. This is similar to the situation in the upper tens of meters in terrestrial ice sheets, and to terrestrial ice caps that have stagnated (e.g. Meighen Ice Cap; Paterson, 1969) or have recently built up (e.g. Hans Tausen Ice Cap; Hvidberg, 2001). A terrestrial ice mass whose slope is determined by the mass-balance pattern alone can take on a much broader range of surface shapes than an ice mass whose slope is determined by a balance between surface mass exchange and ice flow. The two different mass-balance patterns shown in Fig. 4 and in Fig. 5 generate very differently-shaped internal layers, but, as shown in Fig. 5, they produce nearly-identical surfaces.

The inverse method that we used in this paper assumes steady state, so that ice flow, at some rate, has an influence on the topography and on the shapes of internal layers. If an episode of ice flow shaped the North PLD, as proposed by Winebrenner et al. (2008), then our steady-state method is appropriate to infer information about the most recent episode of ice flow. Even in the case of transient flow, transient ice-surface topography resembles steady-state ice-surface topography, but the internal-layer shapes will be different. In the future, we could extend this method using a time-dependent forward algorithm and multiple internal layers, to infer spatial and temporal patterns of accumulation while allowing for transient ice-surface topography. However, as we

have demonstrated here, some fundamental unknowns about the martian PLD can be determined with this simple, steady-state approach.

#### 4.2. Unconformities

Unconformities on various scales have been identified visually in troughs and scarps across the North and South PLD with imagery (e.g. Murray et al., 2002; Tanaka, 2005; Fortezzo and Tanaka, 2006; Kolb and Tanaka, 2006; Tanaka et al., 2008). Subsurface unconformities have also been detected with radar observations (e.g. Seu et al., 2007; Milkovich and Plaut, 2008; Putzig et al., 2009). While unconformities limit the amount of information that we can infer directly from the shape of a deeper internal layer, understanding the cause and timing of these breaks in the stratigraphic record is necessary in order to accurately decipher the history of the PLD and the climate record archived within these deposits.

Fig. 5a shows that an unconformity can develop in steady-state flow when ice moves through multiple zones of accumulation and ablation. Ice is removed in the ablation zone, but ice is deposited on the erosional surface when it moves into the adjacent downstream accumulation zone. This causes spatial gaps in layers of the same age, and causes younger ice to be deposited directly onto much older ice.

### 5. Conclusions

We can successfully solve the inverse problem to infer the spatial variability in mass balance using the shapes of internal layers. Waddington et al. (2007) applied this method to Antarctica, and here we have shown that it is possible to infer spatial patterns of accumulation and ablation, and possibly also the rates of accumulation and ablation, for Mars. While the mass-balance pattern can be inferred, the layer age, the ice velocity, the ice temperature, or the grain size and the crystal fabric must be known before the correct magnitude of the mass-balance rate can be inferred, because steady-state ice-surface topography and layer shapes are, in general, consistent with a wide range of pairs of ice temperature and mass-balance rate magnitude. The ice velocity or ice temperatures necessary in this inverse problem are the values during an era when ice flow closely equilibrated with surface mass balance to produce the surface topography and internal-layer architecture; because the North PLD is probably stagnant today, present-day ice temperatures and accumulation rates are probably not relevant. Therefore, estimating the age of the layer when flow stopped, or determining the ice-grain sizes and conducting laboratory experiments to find the activation energies, ice-softness parameters, and exponents for the ice-flow law on Mars could lead to more appropriate constraints on the mass-balance rate.

Internal layers are necessary to resolve spatial variations in mass balance because surface topography alone retains little of this information. The ice-surface topography can also be inferred from the shape of an internal layer, because there is an ice-surface shape that is consistent with a given mass-balance pattern that together will generate a given internal layer. If the ice temperature at the time of flow is known, then the internal-layer shape and one point on the ice surface can be used to reconstruct the topography. If the ice temperature is unknown, but the internal-layer shape and at least two points widely separated on the ice surface are known, we can also reconstruct the correct topography; this is a problem we can solve with data currently available for Mars. To solve this problem we require internal layers from radar observations that follow putative flowlines. Reconstructed topography across the PLD could be compared to the shape of the present-day ice surface in areas of the PLD that have been significantly altered by trough

formation and other sublimation or deposition processes. Inferring surface topography, mass-balance patterns, and possibly rates and ice temperatures associated with an era of significant ice flow, would be a valuable step towards deciphering the climate history recorded in the PLD.

#### Acknowledgments

We thank T. Neumann for his contributions to the forward and inverse algorithms, and to the original application of this method in Antarctica. We thank A. Pathare, S. Byrne, and B. Murray for stimulating discussions about the martian PLD, and A. Pathare provided helpful comments on an earlier version of this manuscript. We thank two anonymous reviewers for comments that greatly improved the manuscript. This work was supported by the National Science Foundation (NSF, OPP 0440666) and the National Aeronautics and Space Agency (NASA, NNX06AD99G).

#### Appendix A. Forward algorithm

The basis of this algorithm is steady-state continuity (e.g. Paterson, 1994, p. 256),

$$\frac{1}{W(x)} \left( \frac{\partial q(x)}{\partial x} \right) = \dot{b}(x) - \dot{m}(x). \quad (\text{A.1})$$

Along-flow gradients in the volumetric flux of ice  $q(x)$ , in a flowband with surface profile,  $S(x)$ , bedrock profile,  $B(x)$ , and width,  $W(x)$ , must balance the rate of surface accumulation or ablation,  $\dot{b}(x)$ , and any basal melting,  $\dot{m}(x)$ . A time-dependent problem would allow the surface elevation to change over time to accommodate an imbalance in this equality. By integrating Eq. (A.1) from the boundary where ice flux is specified, the ice flux can be represented kinematically by

$$q(x) = q_{in} + \int_{x_{in}}^x (\dot{b}(\zeta) - \dot{m}(\zeta)) W(\zeta) d\zeta, \quad (\text{A.2})$$

where  $q_{in}$  (in  $\text{m}^3 \text{year}^{-1}$ ; we use Earth years) is the ice flux entering at one end of the flowband domain ( $x = x_{in}$ ). An equivalent ice flux can also be represented dynamically, where the flux of ice passing through a cross-sectional area  $W(x) \times H(x)$ , is related to the depth-averaged horizontal velocity  $\bar{u}(x)$  in that cross-section by

$$q(x) = W(x)H(x)\bar{u}(x), \quad (\text{A.3})$$

and  $\bar{u}(x)$  is calculated from the applied gravitational stress together with the constitutive relation for ice. The ice thickness  $H(x) = S(x) - B(x)$ .

The forward algorithm has two components. The first component generates a steady-state ice surface, calculated by equating the ice fluxes,  $q(x)$ , in Eq. (A.2) (kinematic flux) and Eq. (A.3) (dynamic flux). The surface calculation is a dynamic calculation because it incorporates the constitutive relation for strain rate. The second component of the forward algorithm generates internal layers using a kinematic particle-tracking calculation.

In the dynamic calculation, the depth-averaged horizontal velocity comes from the Shallow Ice Approximation (SIA, e.g. Hutter, 1983, p. 256; Paterson, 1994, p. 262). The SIA is a simplifying assumption that applies in cases where the ice thickness is much smaller than the characteristic horizontal length scales over which thickness or stress change significantly. If the characteristic horizontal length scale is the lateral extent of the ice cap, then derivatives of velocities and stresses with respect to  $x$  (horizontal axis) are generally much smaller than derivatives with respect to  $z$  (vertical axis). An extended constitutive relationship for ice flow is given by Eq. (C.1). Here we use the SIA, where  $\tau_{xz}$  is the only important component of stress, and we assume that the linear

term in Eq. (C.1) is negligible. Then, the ice-flow law (Glen, 1955) reduces to

$$\dot{\epsilon}_{xz} = A(T(x, z))\tau_{xz}^n, \quad (\text{A.4})$$

where  $\dot{\epsilon}_{xz} = (1/2)\partial u/\partial z$  is the simple-shear strain rate along a horizontal plane,  $T(x, z)$  is the ice temperature,  $\tau_{xz}$  is the shear stress along a horizontal plane, and based on laboratory experiments  $n$  typically has a value of three for dislocation creep (e.g. Paterson, 1994, p. 85), and  $A(T(x, z))$  is the temperature-dependent softness parameter (in  $\text{Pa}^{-n} \text{year}^{-1}$ ; e.g. Paterson, 1994, p. 86)

$$A(T) = A_0 \exp(-Q/RT), \quad (\text{A.5})$$

where  $A_0$  is the temperature-independent ice-softness parameter,  $Q$  is the activation energy for creep, and  $R$  is the universal gas constant. Using the flow law in Eq. (A.4) and writing shear stress as  $\tau_{xz} = -\rho g(S - z)dS/dx$  using the SLA, and integrating strain rate over depth to get velocity, and integrating again to get the depth-averaged horizontal velocity,

$$\bar{u}(x) = \frac{2\tilde{A}(x)}{n+2} (\rho g)^n \left| \frac{dS}{dx} \right|^{n-1} \left( -\frac{dS}{dx} \right) H^{n+1}(x), \quad (\text{A.6})$$

where  $\rho$  is density,  $g$  is gravitational acceleration,  $S(x)$  is ice-surface elevation,  $H(x)$  is ice thickness, and  $\tilde{A}(x)$  is an effective isothermal softness parameter. The effective isothermal softness parameter is found by equating a depth-averaged ice velocity using a temperature-dependent softness parameter  $A(T(x, z))$ , with depth-varying temperature  $T(x, z)$ , with the depth-averaged ice velocity for an isothermal column at temperature  $T(x)$ , as in Eq. (A.6), and solving for the effective isothermal temperature  $T(x)$ , and corresponding softness parameter  $\tilde{A}(x)$  required to give the same depth-averaged velocity and ice flux.

By representing depth-averaged velocity  $\bar{u}(x)$  in terms of ice flux and ice thickness using Eq. (A.3), and representing ice thickness as the difference between the surface and the known bed elevations,  $H(x) = S(x) - B(x)$ , Eq. (A.6) can be rearranged to produce a non-linear ordinary differential equation for the steady-state ice surface  $S(x)$ ,

$$\frac{dS(x)}{dx} = - \left( \frac{(n+2)q(x)}{2\tilde{A}(x)(\rho g)^n W(x)(S^{n+2}(x) - B^{n+2}(x))} \right)^{1/n}. \quad (\text{A.7})$$

The ice flux,  $q(x)$ , is found kinematically using Eq. (A.2). The ice-surface elevation at one point along the flowband is required as an initial condition to solve Eq. (A.7).

In the calculation used here, the paths of particles starting on the surface are tracked through space and time by integrating the velocity field, given below. We represent the horizontal velocity,  $u(x, z)$ , in terms of its depth-averaged value,  $\bar{u}(x)$ , and a non-dimensional shape function,  $\phi(x, \hat{z})$ , which captures variations with depth (Reeh, 1988),

$$u(x, z) = \bar{u}(x)\phi(x, \hat{z}), \quad (\text{A.8})$$

where  $\hat{z}$  is the normalized non-dimensional height above the bed,

$$\hat{z} = \frac{z - B(x)}{S(x) - B(x)}. \quad (\text{A.9})$$

The choice of the appropriate shape functions  $\phi(x, \hat{z})$  from a thermomechanical calculation can depend on the particular inverse problem being solved. Here we chose to use shape functions for an isothermal, parallel-sided slab (e.g. Paterson, 1994, p. 251).

We invoke mass conservation to find the vertical velocity. Since ice is incompressible,

$$\frac{\partial w}{\partial z} = - \left( \frac{\partial u}{\partial x} + \frac{\partial v}{\partial y} \right), \quad (\text{A.10})$$

where  $u$  is the horizontal velocity along the flowband,  $v$  is the velocity transverse to the central flow line in the flowband as required to make flow tangential to the flowband width, and  $w$  is the vertical velocity. In a flowband, the transverse strain rate (e.g. Paterson, 1994, p. 257) is

$$\frac{\partial v(x, z)}{\partial y} = \frac{1}{W(x)} \frac{dW}{dx} u(x, z). \quad (\text{A.11})$$

The vertical velocity is,

$$w(x, z) = - [\dot{b}(x)\psi(x, \hat{z}) - \dot{m}(x)(1 - \psi(x, \hat{z}))] + u(x, z) \left[ (1 - \hat{z}) \frac{dB}{dX} + \hat{z} \frac{dS}{dx} \right] - \bar{u}(x)H(x) \int_0^{\hat{z}} \frac{\partial \phi(x, \hat{\zeta})}{\partial x} d\hat{\zeta}, \quad (\text{A.12})$$

where

$$\psi(x, \hat{z}) = \int_0^{\hat{z}} \phi(x, \hat{\zeta}) d\hat{\zeta} \quad (\text{A.13})$$

is called the vertical-velocity shape function, and  $\phi(x, \hat{z})$  is called the horizontal-velocity shape function in Eq. (A.8).

The calculated horizontal and vertical velocity fields are then integrated over time to obtain the paths of particles that started on the ice surface. A layer of a particular age is found by connecting the end points of particle paths calculated over a time span equal to the age of the layer. A sequence of steady-state layers subject to the same mass-balance pattern can be generated using a sequence of layer ages.

## Appendix B. Inverse algorithm

For a particular inverse problem with an associated forward algorithm, different inversion procedures should yield similar solutions. Different procedures may have different advantages and disadvantages affecting the accuracy, uniqueness, stability, and computation time. We chose an inverse procedure that is computationally fast and converges on a single solution that satisfies our criterion for an appropriate match to our data.

In an inverse problem, the observable quantities (e.g. internal layers) may not contain enough information to discriminate against solutions (e.g. mass-balance patterns) that are physically unreasonable on other grounds. Because observations contain errors, we do not want to fit these data exactly; a solution found by minimizing only the mismatch between the data and the forward-algorithm prediction could overfit the data. To find a physically reasonable solution, we stabilize, or regularize, the inverse algorithm. As part of this regularization, we require that the mass-balance pattern vary smoothly along the flowband, because variability on small spatial scales is unexpected. Because roughness is penalized, any variability in the solution is clearly required by the data. We also require a solution that fits the data with a root-mean-square mismatch consistent with data uncertainties. The solution to this problem is a “model”, i.e. a vector of the model parameters (e.g. mass-balance rate at discrete points) that we seek. Obtaining a smooth model that fits the data at an expected tolerance can be achieved by minimizing a performance index  $I_p$  given by

$$I_p = \|m\|^2 + v(\|d\|^2 - T^2). \quad (\text{B.1})$$

In this application, the squared model norm,  $\|m\|^2$ , contains the square of the curvature of the accumulation-rate profile integrated along the flowband. For model parameters that do not fall in this

spatial sequence, the model norm incorporates deviations of the inferred values of these parameters from expected values, in which we have a known confidence. Penalizing large values of  $\|m\|^2$  prevents the solution from exhibiting roughness in the accumulation-rate profile or deviating too far from expected values of the other parameters. The squared data norm,  $\|d\|^2$ , is the sum of squared mismatches between the  $N_d$  observations,  $o_i^{(d)}$ , and the forward-algorithm predictions of the same observable quantities,  $o_i^{(m)}$ , normalized by the standard deviations  $\sigma_i^{(d)}$  of the data:

$$\|d\|^2 = \sum_{i=1}^{N_d} \left[ \frac{(o_i^{(m)} - o_i^{(d)})}{\sigma_i^{(d)}} \right]^2 \quad (\text{B.2})$$

The factor  $\nu$  is a trade-off parameter, which is adjusted until the solution produces a data norm that equals a defined tolerance,  $T \sim \sqrt{N}$ , which is based on the statistical uncertainties  $N$  of the data (Parker, 1994, p. 124). The data-mismatch criterion,

$$\|d\|^2 - T^2 = 0, \quad (\text{B.3})$$

is then satisfied. This value of  $\nu$  sets the most appropriate trade-off between smoothness and fit. A smaller value of  $\nu$  puts more emphasis on a smooth model, whereas a larger value of  $\nu$  puts more emphasis on closely fit data (Parker, 1994).

Our inverse method performs a local search for the most-likely solution by finding the minimum of  $I_p$  in the model space that is most accessible from the initial guess of the parameter set. This steepest-descent approach locates only one solution, and that solution may be only a local minimum. To address this issue, we can start from multiple initial guesses of the parameter set. In addition, most inverse problems are non-linear, making them more difficult to solve. Our problem is non-linear because predictions of the data by the forward algorithm are non-linear functions of the model parameters. We address this complication by linearizing our problem. This means that instead of solving for the solution directly, we iteratively solve for corrections to trial values of the unknown parameters. The parameter values are guessed at the first iteration, and are then adjusted in subsequent iterations as the inverse algorithm minimizes the performance index (Eq. (B.1)). The forward algorithm makes predictions of the data using estimates of the model parameters from the previous iteration. For any given value of the trade-off parameter  $\nu$ , a solution is found when adjustments to the model parameters become small. We then adjust the value of  $\nu$  and repeat the solution procedure until the solution also satisfies the data-mismatch criterion (Eq. (B.3)).

Formal inverse theory allows us to investigate our ability to infer unknown parameters; this ability is known as the resolving power. The preferred solution from our regularized algorithm minimizes the performance index  $I_p$  (Eq. (B.1)), and fits the data at an expected tolerance, satisfying Eq. (B.3). However, we still do not know whether we have found the best values and spatial variability of the parameters. It is important to assess the ability to resolve those parameters before making physical inferences from the preferred solution. Parker (1994; pp. 200–213) showed that, when using a regularized algorithm, the inferred structure is a version of the true structure that has been smoothed by a set of narrowly peaked model-resolving functions. The half-width of the resolving function at each spatial position gives the physical scale over which meaningful structure can be resolved. Features with shorter spatial extent than this cannot be resolved with confidence from these data and this algorithm.

### Appendix C. Modified ice-flow law

The modified ice-flow law from Pettit and Waddington (2003), in tensor notation, is

$$\dot{\epsilon}_{ij} = \left[ \frac{E_1 A_{01}}{d^{P_1}} e^{(-Q_1/RT)} + \frac{E_2 A_{02}}{d^{P_2}} e^{(-Q_2/RT)} (\tau_{eff}^2) \right] \tau_{ij}, \quad (\text{C.1})$$

where  $\dot{\epsilon}_{ij}$  is the strain-rate tensor,  $E_1$  and  $E_2$  are the two enhancement factors,  $A_{01}$  and  $A_{02}$  are the two temperature-independent softness parameters,  $d$  is the average grain diameter, exponents  $P_1$  and  $P_2$  express grain-size dependencies,  $Q_1$  and  $Q_2$  are the activation energies for creep,  $R$  is the gas constant,  $\tau_{ij}$  is the deviatoric-stress tensor, and  $\tau_{eff}$  is the effective deviatoric stress ( $\tau_{eff}^2$  is the second tensor invariant of  $\tau_{ij}$ ). The first term in Eq. (C.1) is linear in the deviatoric stress  $\tau_{ij}$ , while the second term is a non-linear (Glen) term with  $n = 3$ . When the coefficient of  $\tau_{eff}^2$  in the second term is extracted as a common factor on the left-hand side of Eq. (C.1), the strain rate  $\dot{\epsilon}_{ij}$  can be expressed as

$$\dot{\epsilon}_{ij} = \Gamma [k^2 + \tau_{eff}^2] \tau_{ij}, \quad (\text{C.2})$$

where  $k$  is called the crossover stress because it is the deviatoric stress at which the linear and non-linear terms contribute equally to the strain rate;  $\Gamma$  is given by

$$\Gamma = \frac{E_2 A_{02}}{d^{P_2}} e^{(-Q_2/RT)}, \quad (\text{C.3})$$

and  $k$  is given by

$$k = \left[ \frac{E_1 A_{01}}{E_2 A_{02}} \frac{d^{P_2}}{d^{P_1}} e^{-\frac{Q_1 - Q_2}{RT}} \right]^{1/2}. \quad (\text{C.4})$$

Pettit and Waddington (2003) showed that a linear constitutive relationship produces an ice divide with a more-rounded (less-peaked) shape. In order to successfully resolve an unknown mass-balance rate and an unknown ice temperature using the additional rate factor in Eq. (C.1), the ice sheet must have been in a regime where the linear and the non-linear terms in Eq. (C.1) have similar magnitudes.

### References

- Aster, R., Borchers, B., Thurber, C., 2005. Parameter Estimation and Inverse Problems. Elsevier Academic Press.
- Barr, A.C., Milkovich, S.M., 2008. Ice grain size and the rheology of the martian polar deposits. *Icarus* 194, 513–518.
- Clifford, S., 1987. Polar basal melting on Mars. *J. Geophys. Res.* 92, 9135–9152.
- Conway, H., Hall, B.L., Denton, G.H., Gades, A.M., Waddington, E.D., 1999. Past and future grounding-line retreat of the West Antarctic ice sheet. *Science* 286, 280–283.
- Durham, W.B., Kirby, S.H., Stern, L.A., 2001. Rheology of ice I at low stress and elevated confining pressure. *J. Geophys. Res.* 106, 11031–11042.
- Fahnestock, M., Abdalati, W., Luo, S., Gogineni, P., 2001. Internal layer tracing and age-depth-accumulation relationships for the Northern Greenland ice sheet. *J. Geophys. Res.* 106 (D24), 33789–33798.
- Fisher, D., 1993. If martian ice caps flow: Ablation mechanisms and appearance. *Icarus* 105, 501–511.
- Fisher, D., 2000. Internal layers in an “accublation” ice cap: A test for flow. *Icarus* 144, 289–294.
- Fortezzo, C.M., Tanaka, K.L., 2006. Unconformity and bedding orientations in Planum Boreum, Mars: Preliminary results and discussion. In: 4th International Conference on Mars Polar Science and Exploration (abstract 8079).
- Glen, J.W., 1955. The creep of polycrystalline ice. *Proc. R. Soc. London A228* (1175), 519–538.
- Greve, R., Mahajan, R.A., Segsneider, J., Grieger, B., 2004. Evolution of the north polar cap of Mars: A modeling study. *Planet. Space Sci.* 52, 775–787.
- Greve, R., Mahajan, R.A., 2005. Influence of ice rheology and dust content on the dynamics of the north-polar cap on Mars. *Icarus* 174, 475–485.
- Grott, M., Helbert, J., Nadalini, R., 2007. Thermal structure of martian soil and the measurability of the planetary heat flow. *J. Geophys. Res.*, 112. doi:10.1029/2007JE002905.
- Goldsbey, D.L., Kohlstedt, D.L., 1997. Grain boundary sliding in fine-grained ice I. *Scripta Mater.* 37 (9), 1399–1406.
- Goldsbey, D.L., Kohlstedt, D.L., 2001. Superplastic deformation of ice: Experimental observations. *J. Geophys. Res.* 106 (B6), 11017–11030.
- Goldsbey, D.L., 2006. Superplastic flow of ice relevant to glacier and ice-sheet mechanics. In: Knight, Peter G. (Ed.), *Glacier Science and Environmental Change*, pp. 308–314.
- Hooke, R., Le, B., 2005. Principles of Glacier Mechanics, second ed. Cambridge University Press.

- Hudleston, P.J., 1976. Recumbent folding in the base of the Barnes ice cap, Baffin Island, Northwest Territories, Canada. *Geol. Soc. Am. Bull.* 87 (12), 1684–1692.
- Hutter, K., 1983. *Theoretical Glaciology*. D. Reidel Publishing, Tokyo, Japan.
- Hvidberg, C.S., 2003. Relationship between topography and flow in the north polar cap on Mars. *Annals Glaciol.* 37, 363–369.
- Hvidberg, C.S., Keller, K., Gundestrup, N., Jonsson, P., 2001. Ice-divide flow at Hans Tausen Iskappe, North Greenland, from surface movement data. *J. Glaciol.* 47 (156), 78–84.
- Jacobson, H.P., Waddington, E.D., 2005. Recumbent folding of divide arches in response to unsteady ice-divide migration. *J. Glaciol.* 51 (173), 201–209.
- Kolb, E., Tanaka, K.L., 2006. Accumulation and erosion of south polar layered deposits in the Promethei Lingula region, Planum Australe, Mars. *Mars* 2, 1–9.
- Koutnik, M.R., Waddington, E.D., Winebrenner, D.P., Neumann, T.A., 2008. Was martian ice warmer in the past? In: LPSC XXXIX (abstract 2293).
- Laskar, J., Levrard, B., Mustard, J., 2002. Orbital forcing of the martian polar layered deposits. *Nature* 419, 375–377.
- Menke, W., 1989. *Geophysical data analysis: Discrete inverse theory*. International Geophysics Series, vol. 45. Academic Press.
- Milkovich, S.M., Plaut, J.J., 2008. Martian south polar layered deposit stratigraphy and implications for accumulation history. *J. Geophys. Res.* 113, E06007. doi:10.1029/2007JE002987.
- Morse, D.L., Waddington, E.D., Steig, E.J., 1998. Ice age storm trajectories inferred from radar stratigraphy at Taylor Dome, Antarctica. *Geophys. Res. Lett.* 25 (17), 3383–3386.
- Murray, B., Koutnik, M., Byrne, S., Soderblom, L., Herkenhoff, K., Tanaka, K., 2002. Preliminary geological assessment of the Northern Edge of Ultimi Lobe, martian South polar layered deposits. *Icarus* 154, 80–97.
- Paren, J.G., Robin, G., de, Q., 1975. Internal reflections in polar ice sheets. *J. Glaciol.* 14 (71), 251–259.
- Parker, R.L., 1994. *Geophysical Inverse Theory*. Princeton University Press, Princeton, NJ.
- Paterson, W.S.B., 1969. The Meighen ice cap, Arctic Canada: Accumulation, ablation and flow. *J. Glaciol.* 8 (51), 341–352.
- Paterson, W.S.B., 1972. Laurentide ice sheet: Estimated volumes during late Wisconsin. *Rev. Geophys. Space Phys.* 10, 885–917.
- Paterson, W.S.B., 1994. *The Physics of Glaciers*, third ed. Pergamon, Oxford.
- Pathare, A.V., Paige, D.A., 2005. The effects of martian orbital variations upon the sublimation and relaxation of north polar troughs and scarps. *Icarus* 174, 419–443.
- Pettit, E.C., Waddington, E.D., 2003. Ice flow at low deviatoric stress. *J. Glaciol.* 49 (166), 359–369.
- Phillips, R.J., and 26 colleagues, 2008. Mars north polar deposits: Stratigraphy, age, and geodynamical response. *Science* 320(5880), 1182–1185.
- Picardi, G., and 33 colleagues, 2005. Radar soundings of the subsurface of Mars. *Science* 310, 1925–1928.
- Plaut, J.J., and 23 colleagues, 2007. Subsurface radar sounding of the south polar layered deposits of Mars. *Science* 316, 92–95.
- Putzig, N.E., Phillips, R.J., Campbell, B.A., Holt, J.W., Plaut, J.J., Carter, L.M., Egan, A.F., Bernardini, F., Safaeinili, A., Seu, R., 2009. Subsurface structure of Planum Boreum from Mars Reconnaissance Orbiter Shallow Radar soundings. *Icarus*, in press. doi:10.1016/j.icarus.2009.07.034.
- Reeh, N., 1988. A flow-line model for calculating the surface profile and the velocity, strain-rate and stress fields in an ice sheet. *J. Glaciol.* 34 (116), 46–54.
- Seu, R., and 51 colleagues, 2007. Accumulation and erosion of Mars' south polar layered deposits. *Science* 317, 1715–1718.
- Tanaka, K.L., 2005. Geology and insolation-driven climatic history of Amazonian north polar materials on Mars. *Nature* 437, 991–994.
- Tanaka, K., Rodriguez, J.A.P., Skinner Jr., J.A., Bourke, M.C., Fortezzo, C.M., Herkenhoff, K.E., Kolb, E.J., Okubo, C.H., 2008. North polar region of Mars: Advances in stratigraphy, structure, and erosional modification. *Icarus* 196, 318–358.
- Thorsteinsson, Throstur, Waddington, E.D., Fletcher, R., 2003. Spatial and temporal scales of anisotropic effects in ice-sheet flow. *Annals Glaciol.* 37, 40–48.
- Waddington, E.D., Bolzan, J.F., Alley, R.B., 2001. Potential for stratigraphic folding near ice-sheet centers. *J. Glaciol.* 47 (159), 639–648.
- Waddington, E.D., Neumann, T.A., Koutnik, M.R., Marshall, H.-P., Morse, D.L., 2007. Inference of accumulation-rate patterns from deep layers in glaciers and ice sheets. *J. Glaciol.* 53 (183), 694–712.
- Winebrenner, D.P., Koutnik, M.R., Waddington, E.D., Pathare, A.V., Murray, B.C., Byrne, S., Bamber, J.L., 2008. Evidence for ice flow prior to trough formation in the martian north polar layered deposits. *Icarus* 195, 90–105.